Molecular Therapy
Oncolytics
Original Article

Single-cell RNA sequencing reveals a strong connection between *Gadd45g* upregulation and oncolytic HSV infection in tumor tissue

Divya Ravirala,[1] Guangsheng Pei,[2] Zhongming Zhao,[2,3] and Xiaoliu Zhang[1]

[1]Center for Nuclear Receptors and Cell Signaling, Department of Biology and Biochemistry, University of Houston, Houston, TX 77204, USA; [2]Center for Precision Health, School of Biomedical Informatics, The University of Texas Health Science Center at Houston, Houston, TX 77030, USA; [3]Human Genetics Center, School of Public Health, The University of Texas Health Science Center at Houston, Houston, TX 77030, USA

The oncolytic effect of virotherapy derives from the intrinsic capability of the applied virus in selectively infecting and killing tumor cells. Although oncolytic viruses of various constructions have been shown to efficiently infect and kill tumor cells *in vitro*, the efficiency of these viruses to exert the same effect on tumor cells within tumor tissues *in vivo* has not been extensively investigated. Here we report our studies using single-cell RNA sequencing to comprehensively analyze the gene expression profile of tumor tissues following herpes simplex virus 2-based oncolytic virotherapy. Our data revealed the extent and cell types within the tumor microenvironment that could be infected by the virus. Moreover, we observed changes in the expression of cellular genes, including antiviral genes, in response to viral infection. One notable gene found to be upregulated significantly in oncolytic virus-infected tumor cells was *Gadd45g*, which is desirable for optimal virus replication. These results not only help reveal the precise infection status of the oncolytic virus *in vivo* but also provide insight that may lead to the development of new strategies to further enhance the therapeutic efficacy of oncolytic virotherapy.

INTRODUCTION

Oncolytic viruses (OVs) are constructed such that they can selectively infect and kill malignant cells without damaging normal cells.[1,2] Indeed, OVs constructed through various mechanisms have been shown to kill tumor cells efficiently *in vitro*; however, their efficiency to infect and kill tumor cells within tumor tissues *in vivo* has not been extensively investigated.[3–5] Compared with *in vitro* settings, several factors can impede OV infection and spread in tumor tissues *in vivo*. First, unlike tumor cell lines that have been maintained in the laboratory for an extended time, tumor cells within tumor tissues are likely more primitive and, hence, less permissive to the replication of OVs. For example, when an oncolytic herpes simplex virus (HSV) was administered to patients with squamous cell carcinoma as a monotherapy, the virus did not replicate significantly inside the injected tumors.[6] Second, unlike *in vitro*-cultured tumor cells, tumor tissues contain many non-malignant cells, such as fibroblasts, endothelial cells, other stromal cells, and immune cells.[7–9] Whether and to what extent OVs can infect these non-malignant cells remains largely unknown. Finally, the replication and spread of OVs *in vivo* are likely affected by intrinsic intracellular factors and extrinsic antiviral immune mechanisms.[10] Comprehensive and detailed knowledge of the status and extent of OV infection within tumor tissues during virotherapy is fundamentally important to interpreting the therapeutic outcome and to designing more effective ways of applying this therapy in the clinic.

To date, only limited and fragmented studies have been reported on determining the OV infection status during *in vivo* virotherapy. Most of these studies were conducted either using immunohistochemical staining or visualization of a marker gene (e.g., green fluorescent protein [GFP]) carried by the oncolytic virus.[11–14] There are several limitations to these studies due to the nature of the methods used. First, only a small portion of tumor samples was used for the detection of oncolytic viral infection (mostly on a thin layer of tissue section). Accordingly, the resultant data may not truly reflect the entire tumor. Second, the methods could not easily identify the cell types in the tumor tissue that were infected by the oncolytic virus. Most importantly, these methods could not reveal the viral gene expression status in specific cell types within the tumor microenvironment, nor could they detect the full repertoire of viral-host interactions.

The unique ability of single-cell RNA sequencing (scRNA-seq) for simultaneous mapping of both cellular and viral transcriptomes in the same cell provides an opportunity to perform unbiased characterization of virus-host interactions in individual cells in tumor tissues,[15] which are often masked at the population level.[16,17] In the current study, we used scRNA-seq to analyze the gene expression profile of tumor tissues comprehensively following HSV-2-based oncolytic virotherapy. Extensive analyses of the resultant data revealed details about the extent of viral infection and the cell types affected within the tumor, as well as the identity of the cellular genes that undergo

Received 30 July 2021; accepted 7 October 2021;
https://doi.org/10.1016/j.omto.2021.10.006.

Correspondence: Xiaoliu Zhang, Center for Nuclear Receptors and Cell Signaling, University of Houston, SERC3004, 3517 Cullen Blvd, Houston, TX 77204, USA.
E-mail: shaunzhang@uh.edu

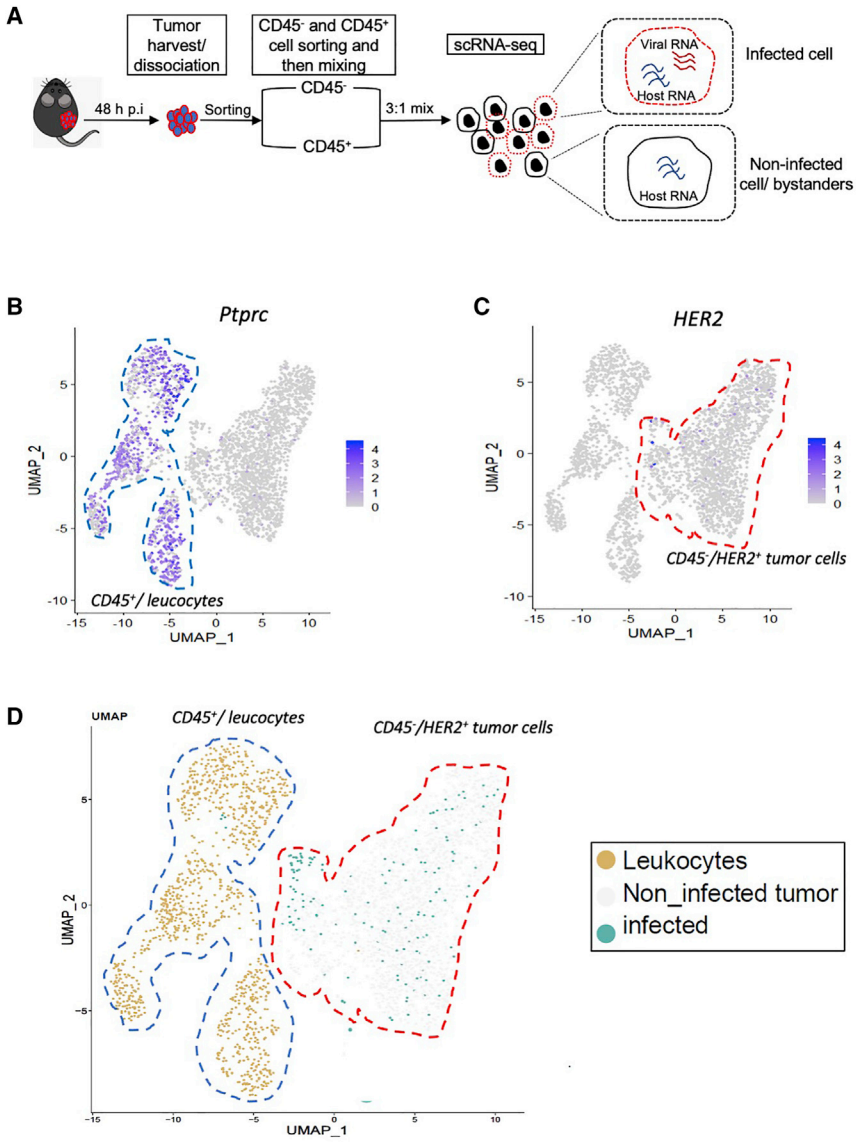

Figure 1. scRNA-seq experiment and data analysis

(A) Tumors were explanted from three mice in each group at 48 h after receiving the FusOn-H3 treatment. Tumors were pooled, digested, and dissociated into single cells, which were subsequently sorted into CD45$^-$ and CD45$^+$ populations and then mixed at a 3:1 ratio for scRNA-seq using a 10× Genomics pipeline. (B and C) Aggregated UMAP of all sequenced cells, classified into immune cells (CD45$^+$/*Ptprc*) and tumor cells (*HER2*$^+$) based on CD45/*Ptprc* (B) and *HER2* (C) expression. (D) Aggregated UMAP plot showing all sequenced cells from both H7 and H7-HER2 groups, classified into leukocytes, non-infected tumor cells, and infected cells based on viral transcript expression.

up- and downregulation in response to viral infection. One of the major findings is that the *growth arrest and DNA-damage-inducible 45 gamma* (*Gadd45g*) gene is significantly upregulated in tumor cells infected by the OV and that this upregulation is desirable for optimal virus replication. These results not only help to reveal the precise infection status and the dynamics of the oncolytic virus *in vivo* but also provide insight into new strategies to further enhance the therapeutic efficacy of oncolytic virotherapy.

RESULTS

scRNA-seq reveals the extent and cell types infected by FusOn-H3 after intratumoral delivery of the OV

The experimental procedure performed in this study is summarized in Figure 1A. Briefly, we established tumors in the right flank of 6- to 8-week-old C57BL/6 mice by implanting an isogenic pair of murine pancreatic cancer cell lines: Panc02-H7 (H7) and Panc02-H7-HER2 (H7-HER2). H7 was derived from the murine pancreatic cell line Panc02,[18] while H7-HER2 was derived from H7 cells stably transduced with a lentiviral vector carrying the coding sequence for human epidermal growth factor receptor 2 (HER2).[19] We included H7-HER2 cells in this experiment because transduction of the *HER2* gene into the cells would allow tumor cells to be annotated based upon the presence of *HER2* transcripts and thus clustered in a Uniform Manifold Approximation and Projection (UMAP) plot. When the tumors reached an approximate size of 8–10 mm in diameter, they were injected with 5×10^6 plaque-forming units (pfu) of FusOn-H3, which was derived by removing the *GFP* gene from FusOn-H2, an HSV-2-based OV.[20] Tumors were collected 48 h post virotherapy, a time point when FusOn-H3 infection/replication reached its peak as revealed by *in vivo* luciferase imaging.[21] The collected tumor tissues were dissociated into a single-cell suspension, which was subsequently sorted into CD45$^-$ and CD45$^+$ populations. CD45$^+$ cells are rare in the tumor microenvironment (TME); therefore, sorting and then mixing them with tumor cells ensured proper representation of both cell populations during sequencing. The CD45$^-$ and CD45$^+$ cells from each tumor sample were mixed at a 3:1 ratio before they were processed for scRNA-seq on the 10× Genomics Chromium controller and then sequenced using the Illumina NextSeq 500 platform at the recommended sequencing depth to provide information for both host and viral gene expression.

The sequencing yielded gene expression profiles from over 3,268 cells in total with a coverage of over 42,609 reads per cell after normalization. The H7 treatment group consisted of 1,314 cells sequenced and 39,215 mean reads per cell, while the H7-HER2 treatment group consisted of 1,954 cells sequenced and 46,003 mean reads per cell. The

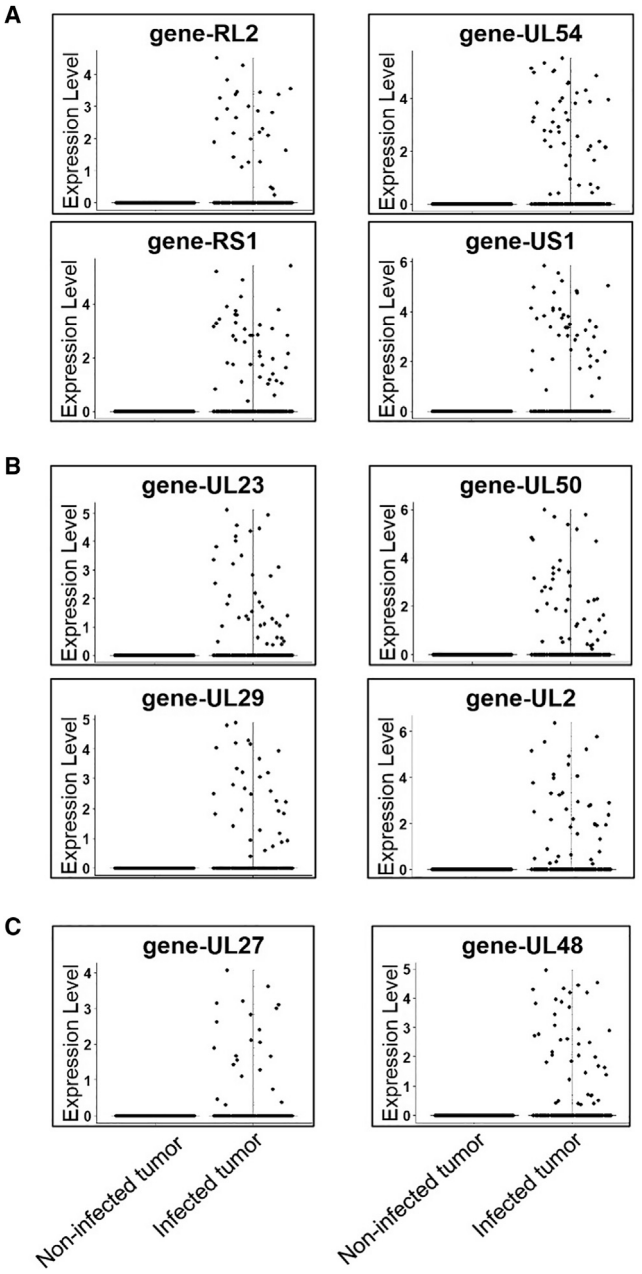

Figure 2. Patterns of the viral gene expression cascade in the infected tumor cells

(A–C) Violin plots showing the expression of representative viral genes from three classes of genes, namely IE (A), E (B), and L (C) genes between infected and non-infected tumor cells.

data were normalized using the Seurat V4.0[22,23] and then combined for subsequent analysis so that tumor cells could be clustered based on the *HER2* transcript in the H7-HER2 population. After clustering and annotation analyses, cells were subsequently classified into two distinct groups: leukocytes (containing all the immune cells) based on CD45 (*Ptprc*) expression (Figure 1B) and tumor cells based on *HER2* expression (Figure 1C). The number of $CD45^{-}/HER2^{+}$ tumor cells (2,163) and $CD45^{+}$ leukocytes (697) was approximately 3:1, matching the ratio that was mixed prior to sequencing. As illustrated in Figure 1A, detection of one or more viral transcripts, regardless of if they are immediate-early (IE), early (E), or late (L) genes, identified the infected cells. In the tumor cell population, approximately 10% (197 infected versus 1,966 non-infected) of tumor cells showed detectable viral transcripts (Figure 1D). However, this value might be an underestimate if infected cells died during or before tumor sample collection, causing their exclusion from flow cytometric sorting.

Leukocytes were reanalyzed at high resolution by sub-clustering immune cells and mapping them to the BlueprintENCODE and Monaco Immune fine reference panels.[24] This analysis yielded five distinct $CD45^{+}$ subpopulations ($CD4^{+}$ and $CD8^{+}$ T cells, B cells, NK cells, neutrophils, and monocytes/macrophages; Figure S1A), which is similar to what we identified in our previous studies on the murine CT26 colon cancer model.[25] In particular, a significant infiltration of B cells (approximately 10% of total infiltrated immune cells) appeared to be a unique feature for this HSV-2-based oncolytic virotherapy. Only a few leukocytes were found to be infected by FusOn-H3, and almost all of them were macrophages (Figures S1B–S1D). These data suggest that, despite intratumor administration at a relatively high dose, FusOn-H2 primarily infected malignant cells within the tumor mass, even though many non-tumor cells, such as leukocytes and other stroma cells, were present.

The cascade of viral gene expression remained relatively consistent in the infected tumor cells

HSV infection in non-neuronal cells (e.g., malignant cells for an OV) usually leads to either a productive lytic infection that results in progeny release and cell death or an abortive infection, in which the cell survives viral infection without generating new viral particles.[26] Thus, characterization of the infection status of tumor cells after *in vivo* delivery of the OV would provide important information about the potential capability of the virus for replication (and spread) within tumors, which is the crux of oncolytic virotherapy.

HSV lytic infection is characterized by an organized cascade of three gene classes, IE (α), E (β), and L (γ) genes.[27] In contrast, abortive infection is limited mainly to IE gene expression with the absence of L gene expression and, consequently, no viral progeny production. Some representative genes from each of the three gene classes are listed in Table S1.

To investigate the gene expression status of the infected tumor cells, we stratified the viral transcripts into genes that represent the three gene classes (IE, E, and L genes). There are only five IE genes. Four of them could be detected by scRNA-seq in this experiment (Figures 2A and S2A). The only IE transcript that could not be detected was *ICP47*, which has been reported to function by binding the TAP transporter to help the virus escape detection by the host immune response.[28] For E and L genes, we focused on those extensively

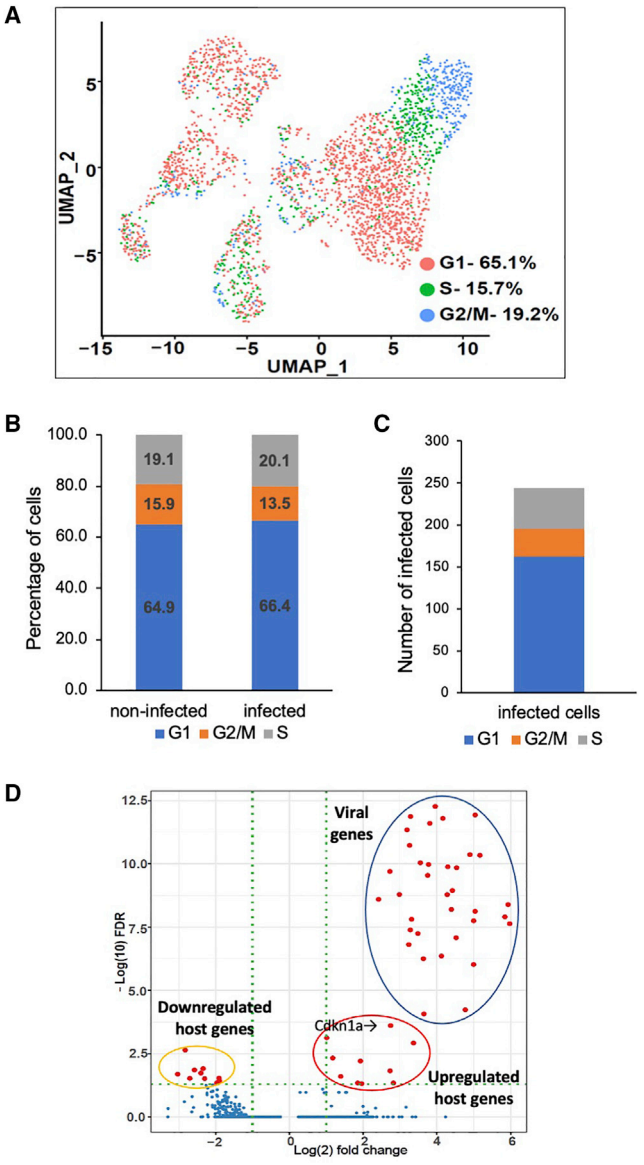

Figure 3. FusOn-H3 infection/replication does not prefer any particular phase in the cell cycle

(A) UMAP plot of cells in different phases of the cell cycle. Cells in G1, G2/M, or S phase are represented in red, blue, or green, respectively. (B) Bar graph showing the percentage of infected and non-infected cells in the G1, G2/M, and S phases. (C) Bar graph showing the absolute number of cells in the G1, G2/M, and S phases of the cell cycle. (D) Volcano plot showing the differentially expressed genes (DEGs) in the high-infected (≥5% of total viral transcripts) versus low-infected cells. Genes in red above the horizontal green dashed line have $p < 0.05$ after false discovery rate (FDR) correction.

investigated by Drayman et al. in their scRNA-seq analysis of an *in vitro* HSV infection.[29] From that list (Table S1), four E genes and two representative L genes are readily detected. The violin plots demonstrate the distribution of these representative genes from the three cascade gene classes (Figures 2B and S2B). Although their distribution among the infected tumor cells varied greatly, the overall distribution patterns of the representative genes were similar across the three gene classes. This indicates that, following infection, gene expression cascade in the tumor cells proceeded without significant disruption. This is in contrast to studies by Drayman et al., which showed that wild-type HSV-1 infection of human fibroblasts resulted in a wide variation of gene expression among individual cells.[29] Notwithstanding the above it is possible that, similar to the total number of the infected cells, the expression of L genes might have been underestimated if infected cells died during or before tumor sample collection.

The total viral transcripts detected by scRNA-seq in the infected tumor cells, which ranged from 0.03% to 42% of the total viral transcripts, are shown in Figure S2. In general, the distribution of viral gene expression was skewed toward the lower end with only approximately 10% of tumor cells expressing a high level of viral transcripts (Figure S2).

The cell-cycle status of FusOn-H3 infected tumor cells

The replication capability of many OVs is closely associated with cell cycling status. FusOn-H3 was constructed such that it preferentially replicates in cells with an activated Ras signaling pathway,[20] which is heavily involved in cell-cycle progression and cell growth.[30] Additionally, studies by Drayman et al. indicate that HSV-1 gene expression was dependent on the cell-cycle stage and that cells at the G2 phase were less likely to initiate viral gene expression.[29] Thus we analyzed the scRNA-seq data to determine the cell-cycle profile of both infected and non-infected tumor cells. The majority of the tumor cells prepared from the explanted tumors were in the G1 phase (Figure 3A). When the infected and non-infected cells were stratified, the same cell-cycle distribution was maintained in both cell populations; i.e., viral infection and gene expression did not exhibit any preference for a specific cell-cycle phase (Figures 3B and 3C). Next, we conducted further analyses on the infected cells by clustering them into either high- or low-infection populations with the threshold of ≥5% of the total viral transcripts to define these two populations. We then analyzed the genes that are either significantly upregulated or downregulated between these two populations and the result is presented as Figure 3D. The results showed that one of the highly upregulated genes in the highly infected cells is cyclin dependent kinase inhibitor 1A (Cdkn1a), which is implicated in the regulation of cell growth and cell response to DNA damage.[31] This may provide a certain linkage to the observed upregulation of *Gadd45g* in the following section. There is no significant difference in all other cell-cycle-associated genes between these two populations. Together, these results indicate that, unlike wild-type HSV infection in normal cells, infection of tumor cells by FusOn-H3 did not prefer any particular phase in the cell cycle for gene expression.

FusOn-H3 infection leads to expression of known antiviral genes in tumor cells

Like many other viruses, HSV infection triggers robust and rapid innate antiviral immune responses aimed at limiting virus

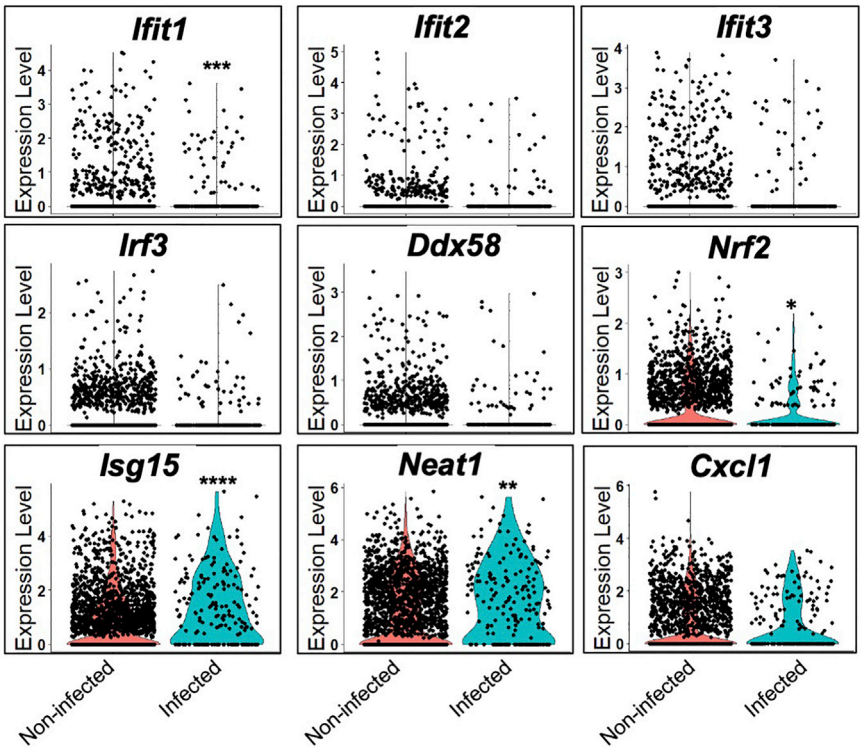

Figure 4. FusOn-H3 infection leads to the expression of known antiviral genes in tumor cells
Violin plots showing the expression of key antiviral genes (*Ifit1*, *Ifit2*, *Ifit3*, *Irf3*, *Ddx58*, *Nr2f2*, *Isg15*, *Neat1*, and *Cxcl1*) in the infected and the non-infected tumor cells. The scale for p values: *p ≤ 0.05, **p ≤ 0.01, ***p ≤ 0.001, ****p ≤ 0.0001.

replication. We thus analyzed the expression of several key antiviral genes, particularly interferon-stimulated genes (Isgs), and examined the potential correlation between transcript abundance and infection status of tumor cells. Three of the Isg genes, *Ifit1* (*Isg56*), *Ifit2* (*Isg54*), and *Ifit3* (*Isg60*), were detected only in a fraction of FusOn-H3 infected cells, with only *Ifit1* showing a significantly higher level of expression in the infected tumor cells (Figure 4). All three are involved in antiviral activities either by selective binding to viral nucleic acids or eukaryotic initiation factor 3 (eIF3) to prevent it from initiating translation.[32] *Irf3*, *Ddx58*, *Neat1*, and *Nr2f2* were also detected in a fraction of the infected tumor cells, with only *Neat1* and *Nr2f2* showing a statistically higher level in the infected tumor cells. *Isg15*, one of the most strongly and rapidly induced Isgs that can directly inhibit viral replication and modulate host immunity,[33,34] was detected at a significantly higher level in FusOn-H3-infected tumor cells. *Cxcl1*, a gene encoding a CXLC chemokine, was also readily detected but the expression level is identical between the infected and non-infected tumor cells. A similar further analysis on the high and low infection clustering on the infected tumor cells as in Figure 3D did not show any significant difference in the expression of these antiviral genes between the two populations.

FusOn-H3 infection in tumor cells is accompanied by significant elevation of *Gadd45g*

In addition to antiviral genes, we analyzed the scRNA-seq data for other cellular genes that were also significantly upregulated in the FusOn-H3-infected cells. The results showed that there were not many. However, *Gadd45g* (also known as *Cr6*, *Ddit2*, *Grp17*, or *Oig37*) was dramatically upregulated in the infected tumor cells compared with non-infected tumor cells, as illustrated by the volcano plot in Figure 5A. *Gadd45g* belongs to the *Gadd45* gene family, which is often induced by DNA damage and other stress signals associated with growth arrest and apoptosis.[35] Interestingly, a recent study by She et al. showed that this gene was significantly upregulated early in wild-type HSV-1-infected cells and that it subsequently acted to facilitate viral replication by suppressing the activation of innate immunity genes.[36] Thus we further examined whether a correlation exists between *Gadd45g* gene expression and FusOn-H3 infection status in tumor cells. We found a notable correlation between *Gadd45g* expression and IE genes (Figure 5B) but a weaker correlation between *Gadd45g* expression and the E and L genes (Figures 5C and 5D). These results indicate that elevated *Gadd45g* expression might play a key role in initiating the early stage of FusOn-H3 infection and a lesser role in the later stages.

Next, we examined the extent of *Gadd45g* expression in both infected and non-infected tumor cells individually. The violin plot in Figure 5E shows that, while only a small fraction of non-infected tumor cells expressed *Gadd45g*, it was overexpressed in 55% (109 of 197) of the infected tumor cells. This result indicates that elevated *Gadd45g* expression is likely due to FusOn-H3-mediated upregulation rather than selective infection of *Gadd45g*-expressing cells. The plot also shows that a significant fraction of the infected tumor cells (45%) did not express this gene or expressed it at a low level, indicating that induction of *Gadd45g* expression by the virus was not ubiquitous.

Interactions of FusOn-H3-infected cells with immune cells in the TME

In addition to lysing tumor cells through infection, OVs can affect the TME indirectly (e.g., by affecting infiltrating immune cells without infecting them). This can result in alteration of the complex intercellular communication networks that exist between immune cells themselves or with tumor cells within the TME. To investigate this, we used CellChat prediction[37] to compare the number of interactions and the interaction strength among

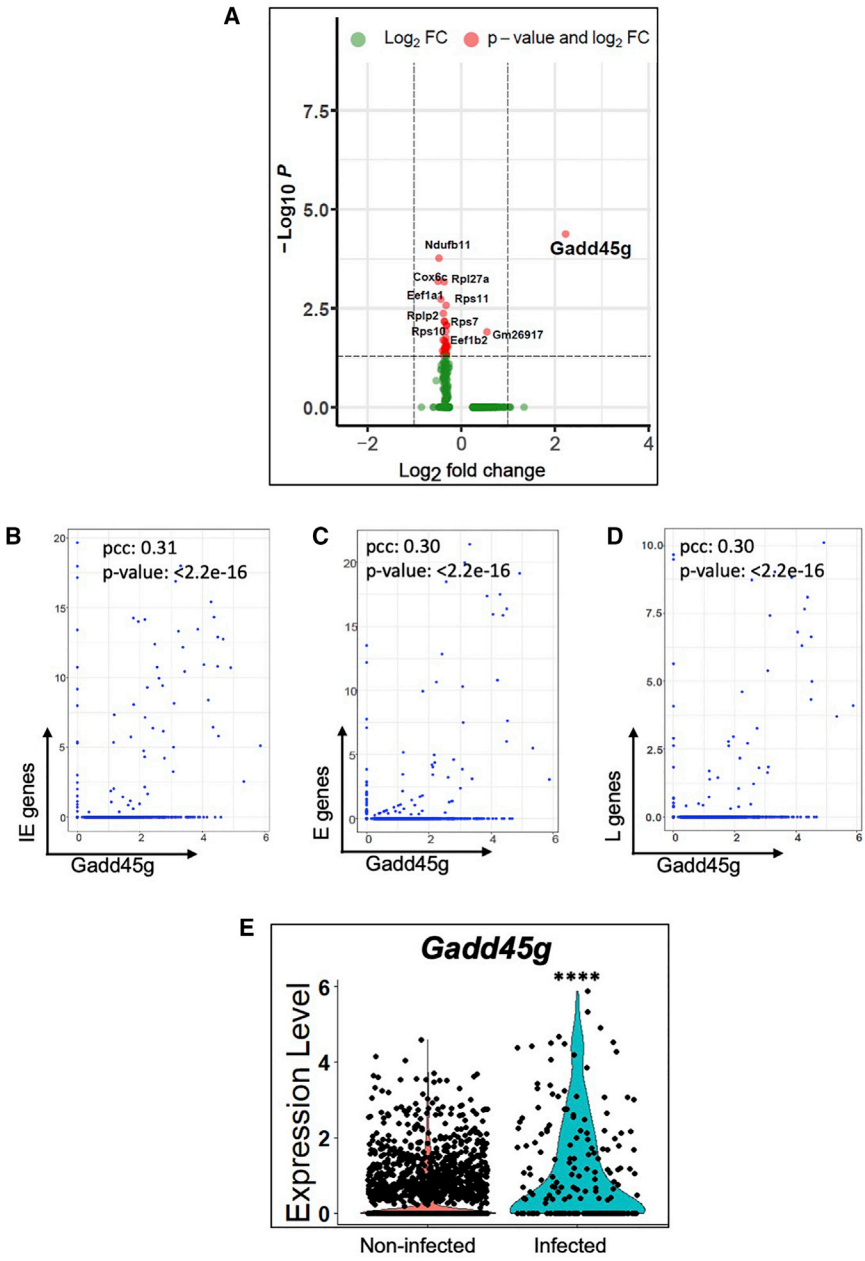

Figure 5. *Gadd45g* expression is significantly increased by FusOn-H3 infection

(A) Volcano plot showing the differential expression of cellular genes in FusOn-H3-infected and non-infected cells. p value ≤ 0.01 for the genes are indicated in red. (B–D) Abundance of viral genes, namely IE (B), E (C), and L genes (D), relative to *Gadd45g* expression. (E) Violin plot showing the expression of *Gadd45g* in infected and non-infected cells ($p \leq 2.8^{-9}$).

different cell populations in infected and non-infected cell populations. Our analysis revealed an increase in the total number of interactions and the interaction strength between FusOn-H3-infected and non-infected cells (Figures 6A and 6B). Based on the predicted interactions of infected and non-infected cells with neighboring immune cells in the TME (Figures 6D and 6E), we can infer that FusOn-H3-infected cells generally displayed a higher level of connectivity and an increased number of interactions between various cell types. In particular, the infected cells had frequent communications with immune cells, including B cells, $CD4^+$ T cells, $CD8^+$ T cells, neutrophils, and macrophages. They were also predicted to communicate with non-infected tumor cells. The predicted CellChat in Figure 6E showing the intensive interaction between infected cells and both innate and adaptive immune cells is not surprising as studies have established that these two immune components need to coordinate to produce an effective immune response against infection or malignancy.[38,39]

Next, we compiled the information flow (i.e., the overall communication probability across the two datasets, infected versus non-infected). This network analysis predicts the information flow for a given signaling pathway that is defined by the sum of the probability of communication between all possible pairs in the inferred network. Intriguingly, 41 out of 77 pathways were found to be highly active, albeit at different levels, in the FusOn-H3-treated group (Figure 6C). Among the pathways showing significantly enhanced information flow upon FusOn-H3 infection were those in the interleukin (IL)-1 family, which consists of 11 cytokines (IL-1α, IL-1β, IL-1Rα, IL-18, IL-33, IL-15, IL-36α, IL-36β, IL-37, IL-38, and IL-36Rα) that collectively play a central role in regulating the immune and inflammatory responses to infection.[40,41] IL-1 family members also have important functions in activating and reinforcing the function of polarized T cells. For example, IL-18 mainly affects T helper (Th) 1 cells, whereas IL-33 affects Th2 cells, and IL-1 plays a key role in Th17 cell differentiation and maintenance.

Effects observed in the H7 pancreatic cancer are largely reproducible in a melanoma tumor model

In order to determine if observations made in Panc02-H7 pancreatic cancer could also be made in solid tumors of epithelial origin, we performed scRNA-seq analysis on tumor samples collected from the murine MC38-HER2 tumor model following FusOn-H3 virotherapy. Some of the collected data are shown in Figure 7. Once again, OV infection was detected mainly in tumor cells with approximately

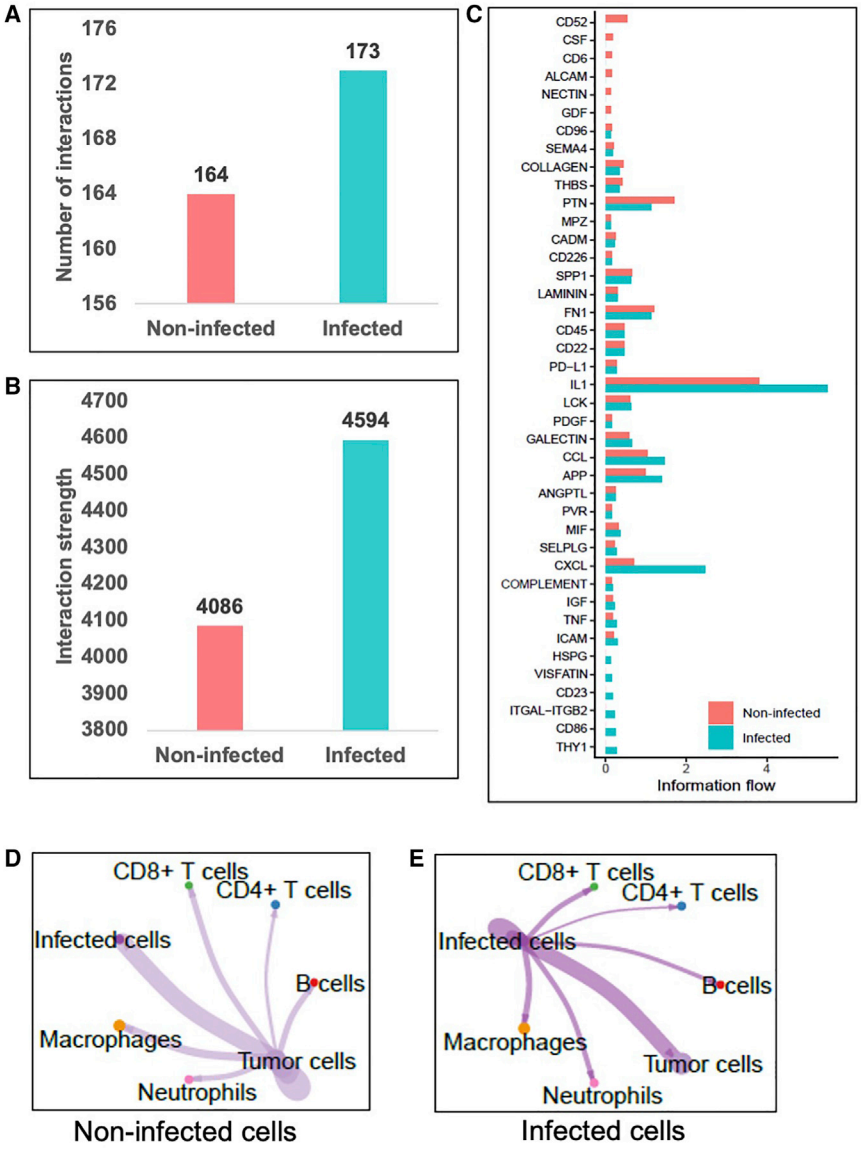

Figure 6. Cell-to-cell communication between infected and non-infected cells in the TME

(A and B) Bar graphs showing the total number of interactions (A) and interaction strength (B) of the inferred cell-cell communication networks between the infected and non-infected cells. (C) Analysis of the signaling pathway networks found to be highly active in either group based on differences in the overall information flow, as predicted by CellChat. (D and E) Summary chord plots showing interactions between the infected (D) and non-infected tumor cells (E) with the neighboring immune and tumor cells.

10% of tumor cells showing viral gene expression (Figure 7A). The majority of tumor cells were in the G1 phase when the tumor samples were collected, and viral gene expression did not show any preferences for a particular cell-cycle phase (Figures 7B and 7C). Viral infection in the tumor cells triggered upregulation of known antiviral genes (*Isg15* and *Cxcl1*), as well as the *Gadd45g* gene (Figure 7D). Together, these results indicate that intratumoral administration of FusOn-H3 in solid tumors of epithelial origin displays a similar viral gene expression pattern and an identical upregulation of cellular gene expression that may provide insight into a new combinatorial therapeutic strategy.

DISCUSSION

The oncolytic effect of virotherapy derives from the ability of the conditionally replicating virus to specifically infect tumor cells *in vivo*. Although most constructed OVs have been shown to efficiently infect tumor cells *in vitro*, their full ability to infect tumor cells *in vivo* remains largely unknown. Unlike *in vitro* settings, OV infection of tumor cells *in vivo* is affected by many additional factors. These include the inability to deliver the virus evenly among the tumor tissues, the presence of tumor stroma that can prevent the virus from spreading, and the host antiviral immune response. The few studies published thus far on OV infection and spread in *in vivo* tumors were mainly conducted using either immunohistochemistry or a marker-gene-containing OV[11–14]; both of these methods cannot measure viral infection across the entire tumor. scRNA-seq has the unique ability to enable profiling of the whole cellular and viral transcriptome in the entire cell population of the TME without bias.[23] However, scRNA-seq had not been used to investigate the infection status of OVs *in vivo* until recently, when Ramelyte et al. used this technique to characterize tumor tissues obtained from fine-needle aspirates of lesions in primary cutaneous B cell lymphoma.[42] Oncolytic virotherapy is mainly being developed as a treatment for carcinomas, which are malignant neoplasms of epithelial origin; therefore, a comprehensive understanding of OV infection status in major targeted tumor types remains to be fully characterized.

Here we used scRNA-seq to characterize the cellular and viral transcriptomes in individual cells prepared from carcinomas (pancreatic cancer and melanoma) that had been treated with an HSV-2-based OV. We found that this HSV-2-based oncolytic virus, FusOn-H3, has very high selectivity for infecting tumor cells *in vivo*. Infection of non-tumor cells in the TME, particularly $CD45^+$ leukocytes, was extremely rare; when it occurred, the infections were exclusive to macrophages. This result is in contrast to reports by Ramelyte et al., which showed that an HSV-1-based T-VEC could efficiently

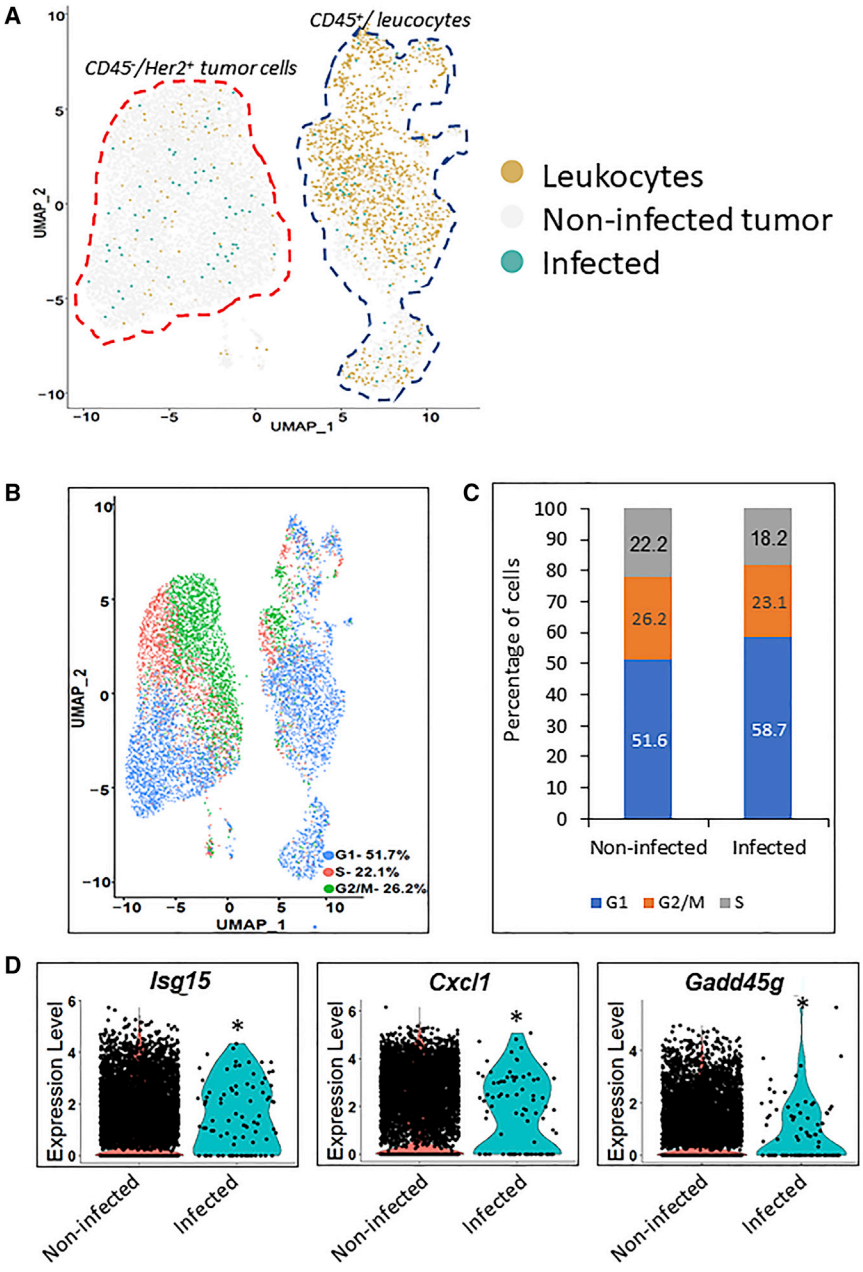

Figure 7. Effect of FusOn-H3 infection on mouse melanoma tumor model

(A–D) C47BL/6 mice (n = 3) bearing either MC38gp100 or MC38gp100HER2 subcutaneous tumors of approximately 8–10 mm were randomly grouped and treated with 5×10^6 pfu FusOn-H3 per mouse. (A) Aggregated UMAP plot depicting all sequenced cells from the MC38gp100 and MC38gp100-HER2 groups classified into leukocytes, non-infected tumor cells, and infected cells based on viral transcript expression. (B) UMAP plot of the cells in different phases of the cell cycle. Cells in G1, G2/M, or S phase are represented in red, blue, and green, respectively. (C) Bar graph showing the percentage of infected and non-infected cells in the G1, G2/M, and S phases. (D) Violin plot showing the expression of *Isg15*, *Cxcl1*, and *Gadd45g* in infected and non-infected cells.

infect malignant B cells and many other immune cells.[42] There are two possible explanations for this apparent discrepancy. First, FusOn-H3 (the original FusOn-H2) and T-VEC were constructed by different mechanisms. The former was constructed such that it selectively targets cells with an activated Ras signaling pathway, while T-VEC was constructed by deleting the *ICP34.5* gene so that the mutant virus preferentially replicates in the dividing cells.[43,44] The different targeting specificity may partly explain the observed differences in cell types infected *in vivo* by these two HSV-based OVs. Second, the source of tumor samples used in these two studies was different, with ours from mice and theirs from humans. Variations in permissiveness to HSV infection between human and mouse immune cells may also explain the differences observed.

Analysis of cellular gene expression status showed that, in addition to upregulation of commonly known antiviral genes, *Gadd45g* was found to be significantly upregulated in the infected tumor cells. Interestingly, a recent study demonstrated that this gene was upregulated in cells infected by wild-type HSV-1 *in vitro*.[36] That study also found that, in contrast to the known antiviral genes that are also frequently upregulated in infected cells, *Gadd45g* facilitates HSV-1 replication by suppressing the activation of a network of innate immunity genes. Further analysis of our scRNA-seq data revealed that *Gadd45g* upregulation following FusOn-H3 infection is not universal at the single-cell level. While FusOn-H3 infection resulted in upregulation of *Gadd45g* expression in many tumor cells, a substantial portion of infected tumor cells still exhibited low or no expression of this gene. This finding, in combination with the report that *Gadd45g* is frequently downregulated in tumor cells,[45] points to the possibility that the replication capability of oncolytic HSV in tumor cells could be enhanced by co-administering a reagent that can enhance this gene expression. As downregulation of *Gadd45g* in tumor cells is found to mainly occur through epigenetic mechanisms,[45] molecules such as decitabine or other hypomethylating agents may be good candidates for a combinatorial treatment. We are currently pursuing this hypothesis by exploring different strategies to overexpress Gadd45g in the remaining tumor cells.

The scRNA-seq studies by Drayman et al. showed that, in human fibroblasts infected by a wild-type HSV-1, viral gene expression

correlated negatively with the cell-cycle score, with cells in the later phases of the cell cycle expressing ~10-fold fewer viral genes than those in the early phases.[29] Our analysis of the cell-cycle profile of both infected and non-infected tumor cells revealed that there was no preference on cell type and gene expression by FusOn-H3 infection in malignant cells. This indicates that although there are many similarities, significant differences can be observed between oncolytic virus infection of malignant cells versus wild-type HSV infection of non-malignant cells.

Despite its unique ability to enable comprehensive and unbiased analyses of transcriptomes from both cellular and viral origins, scRNA-seq has not been used extensively to study OV replication, especially in the *in vivo* experimental settings. In this study, we report results from a comprehensive scRNA-seq analysis of the effect of infection by an HSV-2-based OV in carcinomas. This is the first such study in tumors of epithelial origin. Our findings expand our understanding of the extent and cell types affected by a viral infection in the TME. Additionally, analysis of the cellular gene expression profile of infected tumor cells revealed a potential target to further enhance the therapeutic efficacy of oncolytic virotherapy.

MATERIALS AND METHODS

Cell lines and OVs

H7 was derived from the murine pancreatic cell line Panc02,[18] while H7-HER2 was derived from H7 cells stably transduced with a lentiviral vector carrying the coding sequence for *human epidermal growth factor receptor 2* (*HER2*).[19] The MC38/gp100 cell line was established by stably transducing the murine melanoma cell line MC38 with the human *gp100* gene, as previously described.[46] MC38/gp100-HER2 cells were established by stably transducing MC38/gp100 cells with a lentiviral vector that contains the *HER2* coding sequence. All tumor cells were cultured *in vitro* in Dulbecco's Modified Eagle Medium (Gibco) supplemented with 10% fetal bovine serum (FBS, Gibco).

FusOn-H3, an HSV-2-based oncolytic virus, was originally constructed in our own laboratory and is currently in the process of being translated into clinical application. The virus was constructed by a unique strategy via deleting the N-terminal domain of the *ICP10* gene and replacing it with the GFP gene (for the construction of FusOn-H2). FusOn-H3 was derived from FusOn-H2 by deleting the GFP gene (necessary for clinical application). The details of FusOn-H2 construction and its antitumor properties have been described in our previous studies.[20,47] It has been shown that the N-terminal domain of the *ICP10* gene binds to and phosphorylates the GTPase activating Ras-GDP and turns on the Ras pathway, which is essential for HSV-2 replication.[48] The deletion of this domain region in the *ICP10* gene in FusOn-H2 thus prevents the virus from replicating in the normal cells but allows it to exhibit full replication capability in malignant cells in which the Ras signaling pathway is frequently activated via either *Ras* mutation or downstream activation of other growth factor receptors, such as epidermal growth factor receptor (EGFR).[20,47]

Tumor transplantation and treatment

Immune-competent male C57BL/6 mice (4–6 weeks old) were purchased from Charles River Laboratories. All animal experiments were approved by the university's Institutional Animal Care and Use Committee (IACUC). The right flanks of mice were shaved the day before tumor cell injection. Tumor cells were washed extensively and resuspended in endotoxin-free phosphate-buffered saline (PBS) for tumor implantation in mice. Cells (2×10^5) were then injected subcutaneously into the shaved right flank on the following day. Once the tumor volumes reached an approximate size of 8–10 mm in diameter, mice received an intratumoral injection of FusOn-H3 at a dose of 5×10^6 pfu. Three mice per group (H7, H7-Her2, MC38, and MC38gp100-Her2) were euthanized 48 h after virotherapy to collect tumor tissues for scRNA-seq.

Tumor dissociation and single-cell processing

For scRNA-seq studies, the freshly collected tumors were immediately immersed in a tissue storage medium (Miltenyi, San Diego, CA) and kept at 4°C until ready for dissociation. Within 24 h, tissues were processed into single-cell suspensions using the human Tumor Dissociation Kit from Miltenyi and the gentleMACS Dissociator according to the manufacturer's protocol. Single-cell suspensions were then stained with a fluorophore-conjugated antibody specific to CD45 (BioLegend) for 30 min at 4°C and then washed with cell staining buffer (BioLegend). Live $CD45^+$ cells were sorted on a fluorescence-activated cell sorting (FACS) Melody cell sorter (BD) into 2% FBS in PBS and maintained on ice until further processing for scRNA-seq.

scRNA-seq library preparation and sequencing

Cell suspensions were washed two to four times with PBS and manually counted twice to ensure cell viability was >90% before loading onto the Chromium platform. The libraries were created by successfully capturing cells inside gel beads in emulsion (GEM) by passing cells through a microfluidic channel. Library fragmentation size and quantification were measured before sequencing to ensure that the cDNA was fragmented and barcoded correctly. The cDNA libraries were assessed using an Agilent High Sensitivity 4200 Tapestation system. On the day of single-cell capture and library preparation, the cells were resuspended in PBS containing 0.04% BSA (Ambion, Foster City, CA) to a final concentration of 200 cells/μL. This cell suspension was used as an input for automated single-cell capture and barcoding using the 10× Genomics Full Chromium platform. Approximately 700 single cells were captured for each sample while using the 10× Genomics Single Cell 3′ Chip at the university's Seq-N-Edit Core per standard protocols. The single-cell GEMs were generated and individually barcoded. The cDNA was recovered and selected using DynaBead MyOne Silane Beads (Thermo Fisher Scientific, Carlsbad, CA) and SPRIselect beads (Beckman Coulter, Brea, CA). The sequencing libraries were constructed and quality was assessed using the High Sensitivity 4200 Tapestation system (Agilent, Santa Clara, CA), and the fragments were quantified using a Qubit Fluorometer (Thermo Fisher Scientific, Carlsbad, CA) and Kapa Library Quantification Kit (Kapa Biosystems, Wilmington, MA) with

the AriaMX instrument (Agilent, Santa Clara, CA). The libraries were sequenced on a NextSeq 500 platform (Illumina, San Diego, CA) in stand-alone mode to obtain pair-end sequencing 26 bp (read1) × 98 bp (read2) and a single index 8 bp in length.

scRNA-seq data process

The downstream analysis of scRNA-seq data was performed at the Maxwell cluster high-performance research computing center at the University of Houston using the Cell Ranger 55.0.11 Single Cell Analysis Pipelines (10× Genomics, Pleasanton, CA) analysis software. Raw base call files that were generated by NextSeq 500 were demultiplexed using the cellranger mkfastq function to generate FASTQ files. The reads were aligned to the combined genome reference of mouse (mm10) and human herpesvirus 2 strain HG52 using the cellranger count function. Feature-barcode matrices across different samples were aggregated using the cellranger aggr function, leading to an aggregated read count table.

scRNA-seq data analysis

After constructing the single-cell gene expression count matrix, we used the R package Seurat (v3.1.1)[49] for downstream analysis on the R platform (v3.5.2). Transcription noise cells containing less than 300 genes per cell and/or mitochondrial reads percentage >30% were excluded. All cells passing quality control were merged into one count matrix, normalized, and scaled using Seurat's NormalizeData and ScaleData functions. We assigned each cell a cell phase score based on the expression of G2/M and S phase marker genes using the Seurat CellCycleScoring function. The reduced set of consensus highly variable genes was used as the feature set for independent component analysis on ~3,000 genes using Seurat's RunPCA function. UMAP dimensional reduction was performed on the scaled matrix (with most variable genes only) using the first 40 components of principal component analysis (PCA) to obtain a two-dimensional representation of the cell states. Cell clustering was performed using the FindClusters function, which implements the shared nearest neighbor modularity optimization-based clustering algorithm on 40 PCA components with resolution 0.8, leading to 22 clusters. For each cluster, only the genes that were expressed in >25% of cells with at least 0.25-fold difference were considered marker genes.

To aid in cell type assignment to clusters derived from unsupervised clustering, we performed cell-type enrichment analysis.[50] Cell-type gene signatures were obtained from BlueprintENCODE, and Monaco Immune references from SingleR[51] and human cell landscape.[52] Mouse gene symbols were capitalized to map to human gene symbols. Each gene signature obtained from our clustering was statistically evaluated for overlap with gene signatures contained in these two resources.

Cell-cell communication analysis

To identify and visualize cell-cell interactions between infected and non-infected cells, we employed an R package CellChat.[37] Briefly, we followed the official workflow and loaded the normalized counts into CellChat and applied the standard preprocessing steps, including the functions *identifyOverExpressedGenes*, *identifyOverExpressedInteractions*, and *projectData* with a standard parameter set. A total of 2,021 pre-compiled mouse ligand-receptor interactions were selectively used as *a priori* network information. We then calculated the potential ligand-receptor interactions between infected and non-infected cells based on the functions *computeCommunProb*, *computeCommunProbPathway*, and *aggregateNet* using standard parameters.

Statistical analysis

All quantitative results are displayed as the mean ± SD. The statistical difference between the two groups was determined using the Wilcoxon rank sum statistic in the R software. A p value of less than 0.05 was considered statistically significant.

Data availability

All data needed to evaluate the conclusions in the paper are present in the paper and/or the Supplementary Materials. The raw scRNA-seq data is uploaded to the GEO GSE186753 and will be provided shortly after publication. The materials will be available upon request with a simple MTA.

SUPPLEMENTAL INFORMATION

Supplemental information can be found online at https://doi.org/10.1016/j.omto.2021.10.006.

ACKNOWLEDGMENTS

This work was supported by the Cancer Prevention and Research Institute of Texas (CPRIT) grant RP200464 and a grant from the William and Ella Owens Medical Research Foundation (to X.Z.), the National Institutes of Health grant R01LM012806 (to Z.Z.), and the CPRIT grant RP180734 (to Z.Z.). We thank the University of Houston sequencing core for library construction and sequencing, and Dr. Brandon Mistretta for his assistance with preprocessing and upstream analysis of the scRNA-seq data. We thank Dr. Weiyi Peng for providing the melanoma cell line.

AUTHOR CONTRIBUTIONS

D.R. and X.Z. conceived of the project and designed the experiments. D.R. executed all the experiments in the study. G.P. and D.R. performed bioinformatics analysis. D.R. and X.Z. wrote the manuscript draft. G.P. and Z.Z. helped with data interpretation and finalization of the manuscript.

DECLARATION OF INTERESTS

X.Z. is a co-founder of Tomahawk Oncology.

REFERENCES

1. Lawler, S.E., Speranza, M.-C., Cho, C.-F., and Chiocca, E.A. (2017). Oncolytic viruses in cancer treatment: a review. JAMA Oncol. *3*, 841–849. https://doi.org/10.1001/jamaoncol.2016.2064.

2. Zheng, M., Huang, J., Tong, A., and Yang, H. (2019). Oncolytic viruses for cancer therapy: barriers and recent advances. Mol. Ther. Oncolytics *15*, 234–247.

3. Matuszewska, K., Santry, L.A., van Vloten, J.P., AuYeung, A.W.K., Major, P.P., Lawler, J., Wootton, S.K., Bridle, B.W., and Petrik, J. (2019). Combining vascular normalization with an oncolytic virus enhances immunotherapy in a preclinical

model of advanced-stage ovarian cancer. Clin. Cancer Res. *25*, 1624–1638. https://doi.org/10.1158/1078-0432.Ccr-18-0220.

4. Russell, S.J., Peng, K.W., and Bell, J.C. (2012). Oncolytic virotherapy. Nat. Biotechnol. *30*, 658–670. https://doi.org/10.1038/nbt.2287.

5. Ehrlich, M., and Bacharach, E. (2021). Oncolytic virotherapy: the cancer cell side. Cancers *13*, 393. https://doi.org/10.3390/cancers13050939.

6. Mace, A.T., Ganly, I., Soutar, D.S., and Brown, S.M. (2008). Potential for efficacy of the oncolytic Herpes simplex virus 1716 in patients with oral squamous cell carcinoma. Head Neck *30*, 1045–1051. https://doi.org/10.1002/hed.20840.

7. Strauss, R., and Lieber, A. (2009). Anatomical and physical barriers to tumor targeting with oncolytic adenoviruses in vivo. Curr. Opin. Mol. Ther. *11*, 513–522.

8. Jing, Y., Chavez, V., Khatwani, N., Ban, Y., Espejo, A.P., Chen, X., and Merchan, J.R. (2020). In vivo antitumor activity by dual stromal and tumor-targeted oncolytic measles viruses. Cancer Gene Ther. *27*, 910–922. https://doi.org/10.1038/s41417-020-0171-1.

9. Eriksson, E., Milenova, I., Wenthe, J., Ståhle, M., Leja-Jarblad, J., Ullenhag, G., Dimberg, A., Moreno, R., Alemany, R., and Loskog, A. (2017). Shaping the tumor stroma and sparking immune activation by CD40 and 4-1BB signaling induced by an armed oncolytic virus. Clin. Cancer Res. *23*, 5846–5857. https://doi.org/10.1158/1078-0432.Ccr-17-0285.

10. Wakimoto, H., Johnson, P.R., Knipe, D.M., and Chiocca, E.A. (2003). Effects of innate immunity on herpes simplex virus and its ability to kill tumor cells. Gene Ther. *10*, 983–990.

11. Sauthoff, H., Hu, J., Maca, C., Goldman, M., Heitner, S., Yee, H., Pipiya, T., Rom, W., and Hay, J. (2003). Intratumoral spread of wild-type adenovirus is limited after local injection of human xenograft tumors: virus persists and spreads systemically at late time points. Hum. Gene Ther. *14*, 425–433. https://doi.org/10.1089/104303403321467199.

12. Choi, I.K., Lee, Y.S., Yoo, J.Y., Yoon, A.R., Kim, H., Kim, D.S., Seidler, D.G., Kim, J.H., and Yun, C.O. (2010). Effect of decorin on overcoming the extracellular matrix barrier for oncolytic virotherapy. Gene Ther. *17*, 190–201. https://doi.org/10.1038/gt.2009.142.

13. Thaci, B., Ahmed, A.U., Ulasov, I.V., Tobias, A.L., Han, Y., Aboody, K.S., and Lesniak, M.S. (2012). Pharmacokinetic study of neural stem cell-based cell carrier for oncolytic virotherapy: targeted delivery of the therapeutic payload in an orthotopic brain tumor model. Cancer Gene Ther. *19*, 431–442. https://doi.org/10.1038/cgt.2012.21.

14. Samson, A., Scott, K.J., Taggart, D., West, E.J., Wilson, E., Nuovo, G.J., Thomson, S., Corns, R., Mathew, R.K., Fuller, M.J., et al. (2018). Intravenous delivery of oncolytic reovirus to brain tumor patients immunologically primes for subsequent checkpoint blockade. Sci. Transl. Med. *10*, eaam7577. https://doi.org/10.1126/scitranslmed.aam7577.

15. Jaitin, D.A., Kenigsberg, E., Keren-Shaul, H., Elefant, N., Paul, F., Zaretsky, I., Mildner, A., Cohen, N., Jung, S., Tanay, A., et al. (2014). Massively parallel single-cell RNA-seq for marker-free decomposition of tissues into cell types. Science *343*, 776–779. https://doi.org/10.1126/science.1247651.

16. Steuerman, Y., Cohen, M., Peshes-Yaloz, N., Valadarsky, L., Cohn, O., David, E., Frishberg, A., Mayo, L., Bacharach, E., Amit, I., et al. (2018). Dissection of influenza infection in vivo by single-cell RNA sequencing. Cell Syst. *6*, 679–691.e4. https://doi.org/10.1016/j.cels.2018.05.008.

17. Cristinelli, S., and Ciuffi, A. (2018). The use of single-cell RNA-seq to understand virus-host interactions. Curr. Opin. Virol. *29*, 39–50. https://doi.org/10.1016/j.coviro.2018.03.001.

18. Wang, B., Shi, Q., Abbruzzese, J., Xiong, Q., Le, X., and Xie, K. (2001). A novel, clinically relevant animal model of metastatic pancreatic adenocarcinoma biology and therapy. Int. J. Gastrointest. Cancer *29*, 37–46.

19. Fu, X., Tao, L., Rivera, A., Williamson, S., Song, X.T., Ahmed, N., and Zhang, X. (2010). A simple and sensitive method for measuring tumor-specific T cell cytotoxicity. PLoS One *5*, e11867. https://doi.org/10.1371/journal.pone.0011867.

20. Fu, X., Tao, L., Cai, R., Prigge, J., and Zhang, X. (2006). A mutant type 2 herpes simplex virus deleted for the protein kinase domain of the ICP10 gene is a potent oncolytic virus. Mol. Ther. *13*, 882–890.

21. Fu, X., Tao, L., and Zhang, X. (2018). Genetically coating oncolytic herpes simplex virus with CD47 allows efficient systemic delivery and prolongs virus persistence at tumor site. Oncotarget *9*, 34543–34553. https://doi.org/10.18632/oncotarget.26167.

22. Vieth, B., Parekh, S., Ziegenhain, C., Enard, W., and Hellmann, I. (2019). A systematic evaluation of single cell RNA-seq analysis pipelines. Nat. Commun. *10*, 4667. https://doi.org/10.1038/s41467-019-12266-7.

23. Stuart, T., Butler, A., Hoffman, P., Hafemeister, C., Papalexi, E., Mauck, W.M., 3rd, Hao, Y., Stoeckius, M., Smibert, P., and Satija, R. (2019). Comprehensive integration of single-cell data. Cell *177*, 1888–1902.e21. https://doi.org/10.1016/j.cell.2019.05.031.

24. Monaco, G., Lee, B., Xu, W., Mustafah, S., Hwang, Y.Y., Carre, C., Burdin, N., Visan, L., Ceccarelli, M., Poidinger, M., et al. (2019). RNA-seq signatures normalized by mRNA abundance allow absolute deconvolution of human immune cell types. Cell Rep. *26*, 1627–1640.e7. https://doi.org/10.1016/j.celrep.2019.01.041.

25. Ravirala, D., Mistretta, B., Gunaratne, P., Pei, G., Zhao, Z., and Zhang, X. (2021). Co-delivery of novel bi-specific and tri-specific engagers by an amplicon vector augments the therapeutic effect of a HSV-based oncolytic virotherapy. J. Immuno Ther. Cancer *9*, e002454.

26. Aurelian, L., and Roizman, B. (1965). Abortive infection of canine cells by herpes simplex virus: II. Alternative suppression of synthesis of interferon and viral constituents. J. Mol. Biol. *11*, 539–548.

27. Roizman, B., and Sears, A.E. (1996). Herpes simplex viruses and their replication. In Virology, B.N. Fields, ed. (Raven Press, Ltd.), pp. 541–553.

28. Hill, A., Jugovic, P., York, I., Russ, G., Bennink, J., Yewdell, J., Ploegh, H., and Johnson, D. (1995). Herpes simplex virus turns off the TAP to evade host immunity. Nature *375*, 411–415.

29. Drayman, N., Patel, P., Vistain, L., and Tay, S. (2019). HSV-1 single-cell analysis reveals the activation of anti-viral and developmental programs in distinct sub-populations. eLife *8*, e46339. https://doi.org/10.7554/eLife.46339.

30. Coleman, M.L., Marshall, C.J., and Olson, M.F. (2004). RAS and RHO GTPases in G1-phase cell-cycle regulation. Nat. Rev. Mol. Cell Biol. *5*, 355–366. https://doi.org/10.1038/nrm1365.

31. Cazzalini, O., Scovassi, A.I., Savio, M., Stivala, L.A., and Prosperi, E. (2010). Multiple roles of the cell cycle inhibitor p21(CDKN1A) in the DNA damage response. Mutat. Res. *704*, 12–20. https://doi.org/10.1016/j.mrrev.2010.01.009.

32. Diamond, M.S., and Farzan, M. (2013). The broad-spectrum antiviral functions of IFIT and IFITM proteins. Nat. Rev. Immunol. *13*, 46–57. https://doi.org/10.1038/nri3344.

33. Morales, D.J., and Lenschow, D.J. (2013). The antiviral activities of ISG15. J. Mol. Biol. *425*, 4995–5008. https://doi.org/10.1016/j.jmb.2013.09.041.

34. Swaim, C.D., Scott, A.F., Canadeo, L.A., and Huibregtse, J.M. (2017). Extracellular ISG15 signals cytokine secretion through the LFA-1 integrin receptor. Mol. Cell *68*, 581–590.e5. https://doi.org/10.1016/j.molcel.2017.10.003.

35. Salvador, J.M., Brown-Clay, J.D., and Fornace, A.J., Jr. (2013). Gadd45 in stress signaling, cell cycle control, and apoptosis. Adv. Exp. Med. Biol. *793*, 1–19. https://doi.org/10.1007/978-1-4614-8289-5_1.

36. She, M., Jiang, H., Chen, X., Chen, X., Liu, X., Zhang, X., Roizman, B., and Zhou, G.G. (2019). GADD45γ activated early in the course of herpes simplex virus 1 infection suppresses the activation of a network of innate immunity genes. J. Virol. *93*. https://doi.org/10.1128/jvi.02201-18.

37. Jin, S., Guerrero-Juarez, C.F., Zhang, L., Chang, I., Ramos, R., Kuan, C.-H., Myung, P., Plikus, M.V., and Nie, Q. (2021). Inference and analysis of cell-cell communication using CellChat. Nat. Commun. *12*, 1088. https://doi.org/10.1038/s41467-021-21246-9.

38. Janssen, L.M.E., Ramsay, E.E., Logsdon, C.D., and Overwijk, W.W. (2017). The immune system in cancer metastasis: friend or foe? J. Immunother. Cancer *5*, 79. https://doi.org/10.1186/s40425-017-0283-9.

39. Brucher, B.L., and Jamall, I.S. (2014). Cell-cell communication in the tumor microenvironment, carcinogenesis, and anticancer treatment. Cell. Physiol. Biochem. *34*, 213–243. https://doi.org/10.1159/000362978.

40. Sims, J.E., and Smith, D.E. (2010). The IL-1 family: regulators of immunity. Nat. Rev. Immunol. *10*, 89–102. https://doi.org/10.1038/nri2691.

41. Xu, D., Mu, R., and Wei, X. (2019). The roles of IL-1 family cytokines in the pathogenesis of systemic sclerosis. Front. Immunol. *10*, 2025. https://doi.org/10.3389/fimmu.2019.02025.

42. Ramelyte, E., Tastanova, A., Balazs, Z., Ignatova, D., Turko, P., Menzel, U., Guenova, E., Beisel, C., Krauthammer, M., Levesque, M.P., et al. (2021). Oncolytic virotherapy-mediated anti-tumor response: a single-cell perspective. Cancer Cell *39*, 394–406.e4. https://doi.org/10.1016/j.ccell.2020.12.022.

43. Martuza, R.L., Malick, A., Markert, J.M., Ruffner, K.L., and Coen, D.M. (1991). Experimental therapy of human glioma by means of a genetically engineered virus mutant. Science *252*, 854–856.

44. Liu, B.L., Robinson, M., Han, Z.Q., Branston, R.H., English, C., Reay, P., McGrath, Y., Thomas, S.K., Thornton, M., Bullock, P., et al. (2003). ICP34.5 deleted herpes simplex virus with enhanced oncolytic, immune stimulating, and anti-tumour properties. Gene Ther. *10*, 292–303. https://doi.org/10.1038/sj.gt.3301885.

45. Ying, J., Srivastava, G., Hsieh, W.S., Gao, Z., Murray, P., Liao, S.K., Ambinder, R., and Tao, Q. (2005). The stress-responsive gene GADD45G is a functional tumor suppressor, with its response to environmental stresses frequently disrupted epigenetically in multiple tumors. Clin. Cancer Res. *11*, 6442–6449. https://doi.org/10.1158/1078-0432.Ccr-05-0267.

46. Peng, W., Ye, Y., Rabinovich, B.A., Liu, C., Lou, Y., Zhang, M., Whittington, M., Yang, Y., Overwijk, W.W., Lizée, G., et al. (2010). Transduction of tumor-specific T cells with CXCR2 chemokine receptor improves migration to tumor and antitumor immune responses. Clin. Cancer Res. *16*, 5458–5468. https://doi.org/10.1158/1078-0432.Ccr-10-0712.

47. Fu, X., Tao, L., Li, M., Fisher, W.E., and Zhang, X. (2006). Effective treatment of pancreatic cancer xenografts with a conditionally replicating virus derived from type 2 herpes simplex virus. Clin. Cancer Res. *12*, 3152–3157.

48. Smith, C.C., Nelson, J., Aurelian, L., Gober, M., and Goswami, B.B. (2000). Ras-GAP binding and phosphorylation by herpes simplex virus type 2 RR1 PK (ICP10) and activation of the Ras/MEK/MAPK mitogenic pathway are required for timely onset of virus growth. J. Virol. *74*, 10417–10429.

49. Butler, A., Hoffman, P., Smibert, P., Papalexi, E., and Satija, R. (2018). Integrating single-cell transcriptomic data across different conditions, technologies, and species. Nat. Biotechnol. *36*, 411–420. https://doi.org/10.1038/nbt.4096.

50. Pei, G., Yan, F., Simon, L.M., Dai, Y., Jia, P., and Zhao, Z. (2021). *deCS*: a tool for systematic cell type annotations of single-cell RNA sequencing data among human tissues. bioRxiv *2009*, 460993. https://doi.org/10.1101/2021.09.19.460993.

51. Aran, D., Looney, A.P., Liu, L., Wu, E., Fong, V., Hsu, A., Chak, S., Naikawadi, R.P., Wolters, P.J., Abate, A.R., et al. (2019). Reference-based analysis of lung single-cell sequencing reveals a transitional profibrotic macrophage. Nat. Immunol. *20*, 163–172. https://doi.org/10.1038/s41590-018-0276-y.

52. Liao, M., Liu, Y., Yuan, J., Wen, Y., Xu, G., Zhao, J., Cheng, L., Li, J., Wang, X., Wang, F., et al. (2020). Single-cell landscape of bronchoalveolar immune cells in patients with COVID-19. Nat. Med. *26*, 842–844. https://doi.org/10.1038/s41591-020-0901-9.